Int J Adv Manuf Technol (2015) 77:235–240
DOI 10.1007/s00170-014-6458-3

ORIGINAL ARTICLE

Thermal analysis of chip formation using FEM and a hybrid explicit-implicit approach

R. T. Coelho · J. F. G. de Oliveira · Claudia Hespanholo Nascimento

Received: 15 January 2014 / Accepted: 9 July 2014 / Published online: 12 October 2014

Abstract Modeling machining operations has been a challenge since the 1900s. It has been by empirical, science-based, and computer-based modeling, which started with FEM by the 1970s. For success material, rupture, friction, and convection have to be correctly modeled. Computation time has always been one of the main limitations for accurately describing heat propagation on machining. The present work proposes and tests a hybrid model using an explicit algorithm for the chip formation and an implicit one for heat propagation. Heat flux on workpiece and tool were obtained by the explicit and used as input to the implicit. Simulated results were in good agreement with experimental end milling for very short periods of computer time.

Keywords FEM simulation · Machining · Heat propagation · Convection

1 Introduction

Modeling machining operations have always been around since the beginning of the twentieth century evolving through three main stages: empirical modeling, science-based (predictive), and computer-based [1]. The main objectives have always been the development of predictive capability for machining performance in order to facilitate effective planning of machining operation to achieve optimum productivity, quality, and cost [2]. Empirical models, or semiempirical ones, started in the early 1900s with F.W. Taylor. Resulting equations were very simple, but still very useful, such as that relating tool life and cutting speed. Simple observations, however, and attempts to understand the chip formation process have been made earlier by Tresca in 1873 [3]. During the 1940s, Merchant proposed a physics-based modeling starting at the second stage. The main concepts were the shear plane and the consideration of the chip as a body in stable mechanical equilibrium between the shear plane and the tool face defining the force system acting in the chip-tool-workpiece system. Minimum energy, material failure criterion, and slip line concepts followed. The third stage, around the 1970s, marks the introduction of computers to solve some of the complex models created in the previous two stages. Hardware and software combined created an unprecedented possibility of integrating all those previous models and also to solve and explore new models, especially those based on finite element method (FEM). Arbitrary Lagrangian-Eulerian (ALE) technique was also used to study the temperature at the interface chip-tool explaining tool coating experimental results when machining hardened steel with coated PcBN tools [4]. With ALE, the material flows around the cutting edge and there is no need for material failure criterion, as well as remeshing and contour smoothing techniques [5]. Even high-speed cutting has been successfully simulated by FEM codes in aluminum and titanium alloys [6, 7].

Material constitutive models for FEM simulation have to be a function of strain (ε), strain rate ($\dot{\varepsilon}$), and also temperature (θ), strongly affecting the output results on force and thermal distribution [8]. Many works have been proving that point for the same FEM code and also for different ones [9–12].

Fracture of ductile metals is strongly dependent on the stress triaxiality, which is the ratio of the mean stress by the equivalent one [13]. Commercial nonlinear FE codes normally offer a number of different, ever more sophisticated fracture options, but each criterion is more suitable for a particular application and some fracture parameters have to be determined from a minimum number of tests [14].

R. T. Coelho · C. H. Nascimento (✉)
School of Engineering at São Carlos, The University of São Paulo, São Paulo, SP, Brazil
e-mail: clau.nas271@gmail.com

J. F. G. de Oliveira
The Institute of Technological Research, São Paulo, SP, Brazil

Table 1 Johnson-Cook Constants for stress and failure [4]

AISI	A	B	C	n	m	d_1	d_2	d_3	d_4	d_5	Melting (K)	Transition (K)
4,340	792	510	0.014	0.26	1.03	0.05	3.44	−2.12	0.002	0.61	1793	305

One of the most relevant aspects in thermal analysis is the friction as being the main heat source on the rake face. Several models have been proposed, but none of them seems to be the most effective [15].

Another problem related to the temperature modeling is the cutting time. By using the updated Lagrangian formulation, only few milliseconds of cutting time can be simulated, even in the case of 2D simulations for simple cutting. This aspect is a limit for the modeling since thermal steady state can be achieved only after some seconds of material removal [16]. In addition, there is the convection coefficient (***h***), which controls the loss of heat to the environment [17]. Simulations running for just few seconds do not allow the heat to fully spread and reach stable conditions. The parameter ***h*** also is known to be strongly dependent on the cutting fluid (air, liquid, or mix of both), workpiece/chip surface temperature, as well as the application technique (flooding, compressed air, MQL, etc.) [18].

The present work is concerned with modeling the temperature distribution in metal cutting using FEM. It uses an explicit algorithm to accurately simulate the chip formation, an implicit one to simulate the heat propagation on the workpiece and tool edge together with an experimental procedure to evaluate the convection coefficient [19]. The simulated results are assessed by real milling experiments measuring temperature with embedded thermocouples.

Table 2 Material physical properties [4]

AISI 4340	
Thermal conductivity (W/mK)	38
Coefficient of thermal expansion (μm/m°C)	0.000032
Density (kg/m^3)	7,838
Young's modulus (GPa)	200
Poisson ratio	0.29
Specific heat (J/kg/K)	477
Carbide	
Thermal conductivity (W/mK)	20
Density (Kg/m^3)	14,950
Young's modulus (GPa)	400
Poisson ratio	0.21
Specific Heat (J/kg/°C)	210

2 Description of the model

The first part of the simulation process uses a 2D model solved by an explicit algorithm based upon the implementation of an integration rule together with the use of diagonal or "lumped" element mass matrices. The equations of motion for the body are integrated using the central difference integration rule, given as follows:

$$u^{\left(i+\frac{1}{2}\right)} = u^{\left(i-\frac{1}{2}\right)} + \frac{\Delta t^{(i+1)} + \Delta t^{(i)}}{2}\ddot{u}^{(i)}s \tag{1}$$

$$u^{(i+1)} = u^{(i)} + \Delta t^{(i+1)} u^{\left(i+\frac{1}{2}\right)} \tag{2}$$

Where u is velocity and u is acceleration. The subscript ***i*** is the increment number and $\left(i \pm \frac{1}{2}\right)$ is the mid-increment values. The acceleration is given as follows:

$$\ddot{u} = M^{-1} \cdot \left(F^{(i)} - I^{(i)}\right) \tag{3}$$

where ***M*** is the diagonal lumped mass matrix, ***F*** is the applied load vector, and ***I*** is the internal force vector. The central difference operator is not self-starting and the other conditions are defined as follows:

$$u^{(i+1)} = u^{\left(i+\frac{1}{2}\right)} + \frac{1}{2}\Delta t^{(i+1)}\ddot{u}^{(i+1)} \tag{4}$$

$$u^{\left(\frac{1}{2}\right)} = u^{(0)} + \frac{\Delta t^{(1)}}{2}\ddot{u}^{(0)} \tag{5}$$

$$u^{\left(-\frac{1}{2}\right)} = u^{(0)} - \frac{\Delta t^{(1)}}{2}\ddot{u}^{(0)} \tag{6}$$

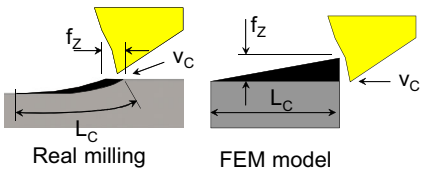

Fig. 1 Schematic of the model for chip formation

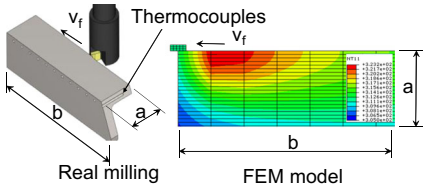

Fig. 2 Geometric model used for the implicit algorithm (*a* 21 mm, *b* 80 mm)

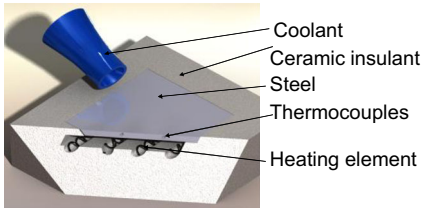

Fig. 3 Experimental set used to evaluate the convection coefficient as a function of the cooling system

The initial values (at time t=0) of velocity and acceleration are set to zero unless they are specified by the user of the ABAQUS™ computer code. For the thermal coupled part of the solution, the equations are integrated using the explicit forward-difference time integration rule:

$$\theta^N_{(i+1)} = \theta^N_{(i)} + \Delta t_{(i+1)} \dot{\theta}^N_{(i)} \tag{7}$$

where θ^N is the temperature at node N. The forward-difference integration is explicit in the sense that no equations need to be solved when a lumped capacitance matrix is used. The current temperatures are obtained using known values of $\dot{\theta}^N_{(i)}$ from the previous increment. The values of $\theta^N_{(i)}$ are computed at the beginning of the increment by:

$$\theta^N_{(i)} = \left(C^{NJ}\right)^{-1}\left(P^J_{(i)} - F^J_{(i)}\right) \tag{8}$$

where C^{NJ} is the lumped capacitance matrix, P^J is the applied nodal source vector, and F^J is the internal flux vector. No heat loss to the ambient was accounted here, since the contact time was too short. The material and the failure were modeled according to Johnson-Cook and the constants are in Table 1 [4].

The other material physical properties used are in Table 2. Figure 1 shows a schematic of the model and a FEM simulation for the chip formation.

This first simulation exactly matches the interaction between cutting edge and workpiece in a single cut of the end mill. The input to the second simulation is the heat flux going into the workpiece, which is given by:

Table 3 Cutting conditions used for the simulations and also for the experimental trials

v_c (m/min)	f_z (m/edge)	n (rpm)	v_f (mm/min)	a_p (mm)	a_e (mm)
80	0.17	1,592	270	5	0.55
100	0.17	1,990	338	5	0.55
150	0.17	2,984	508	5	0.55

$$\bar{Q}_{W,T} = \left(\frac{t_c}{t_{\mathrm{Rev}}}\right)\frac{1}{\Delta t}\int_{\Delta t} q_{W,T}\,dt$$

Where $\overline{Q}_{W,T}$ is the average heat flowing into the workpiece, or tool, for the second simulation, $q_{W,T}$ is the equivalent from the first simulation, t_c is the contact time, and t_{Rev} is the time for one revolution. The values of $q_{W,T}$ were obtained at the centroid of elements on the first layer in the newly cut surface after finishing the analysis. The same procedure was used to cross-check on the second simulation. At this simulation, the heat coming from the plastic deformation and from the friction at the interfaces was accounted for, according to Eqs. (9) and (10):

$$r^{pl} = \eta\sigma : \varepsilon^{pl} \tag{9}$$

$$q_g = \eta\tau\frac{\Delta s}{\Delta t} \tag{10}$$

where r^{pl} is the heat flux that is added into the thermal energy balance, η is a user-defined factor (assumed as 0.9), σ is the normal stress, ε^{pl} is the rate of plastic straining, τ is the frictional stress, and Δs is the incremental slip.

Using $\overline{Q}_{W,T}$ as input, the implicit simulation ran for as long as needed to match the real cutting time and 10 s of cooling time after cutting. Figure 2 shows the geometry of the model.

The implicit algorithm integrates by using a backward-difference scheme, and the nonlinear coupled system is solved using Newton's method. It involves a nonsymmetric Jacobian matrix as illustrated in the following matrix representation of the coupled equations:

$$\begin{bmatrix} K_{uu} & K_{u\theta} \\ K_{\theta u} & K_{\theta\theta} \end{bmatrix}\begin{Bmatrix} \Delta u \\ \Delta\theta \end{Bmatrix} = \begin{Bmatrix} R_u \\ R_\theta \end{Bmatrix} \tag{11}$$

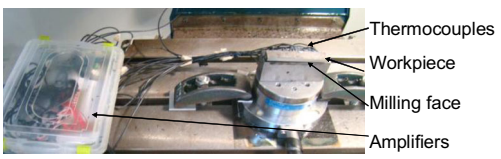

Fig. 4 Schematic of the end mill experiments

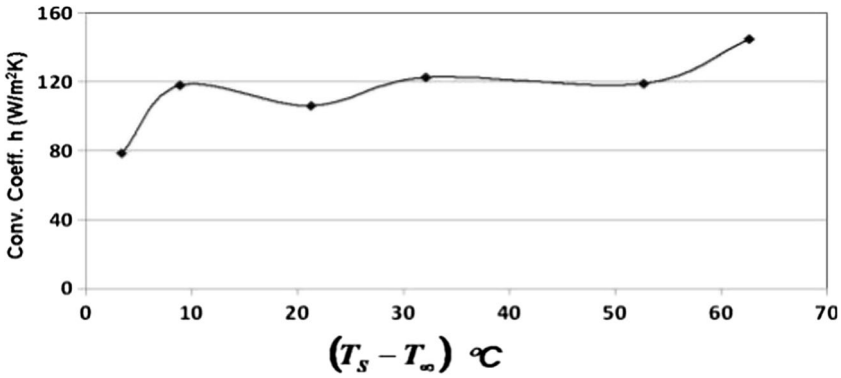

Fig. 5 Experimental results of the convection coefficient (h) as a function of surface rise in temperature

Where Δu and $\Delta\theta$ are the respective corrections to the incremental displacement and temperature, K_{ij} are submatrices of the fully coupled Jacobian matrix, and R_u and R_θ are the mechanical and thermal residual vectors, respectively. The transient analysis was used for the present case. The simulations were run in three different cutting conditions, according to Table 3, as well as the experimental end milling trials.

At this second simulation, the convection effect was introduced and values of the convection coefficient (***h***) were needed. Equation (12) was used, in an experimental set up:

$$h = \frac{q}{A(T_S - T_\infty)} \tag{12}$$

Where q is the heat flowing from the heated surface into the surrounding fluid, ***h*** is the convection coefficient, ***A*** is the area perpendicular to the flux, $\boldsymbol{T_s}$ is the surface temperature, and T_∞ is the fluid temperature. A small plate of steel was fitted into a ceramic insulation material (Al_2O_3). It contained three embedded thermocouples and a heating element below. The heat flowing through the plate was admitted to equal the total electric power, calculated as follows:

$$P = U \cdot I \tag{13}$$

where ***P*** is the electric power, ***U*** is the continuous voltage, and ***I*** is the electric current. Figure 3 shows a schematic of that experiment.

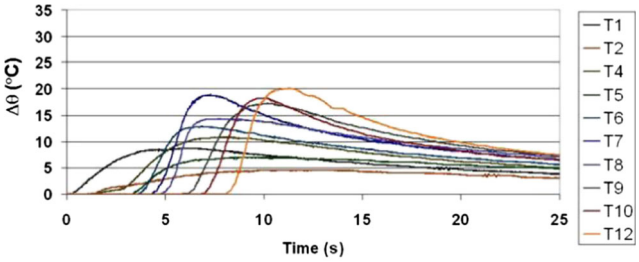

(a) Experimental results

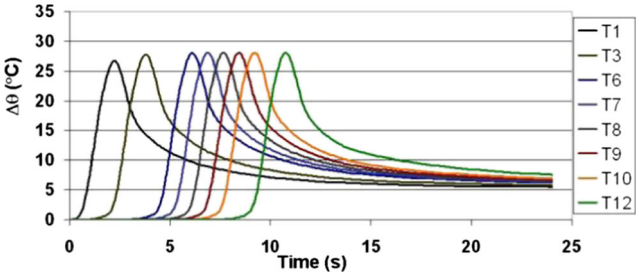

(b) Simulated results

Fig. 6 Experimental and simulated temperature rise for $\boldsymbol{v_c}$=80 m/min and $\boldsymbol{f}$=0.17 mm/rev

3 Experimental work

The end milling experiments consisted of running end milling operations on hardened AISI4340 (48–50 HRc) on 2D force arrangement, as shown in Fig. 4.

One single end milling insert code R390-11 T308M-PL 1030 was used on a R390-016A16-11 L, a 16-mm diameter shank. Its cutting edge profile was accurately measured to input into the FEM simulation.

The experimental temperature was measured with embedded 12 pieces of K-type thermocouples embedded and equally spaced at 4.5 mm apart, as shown in Fig. 2 [20–22]. Measurements were taken at 0.55 mm from the milled plan. Simulated results were compared with the experimental ones in two ways. The first one was to compare the curves individually

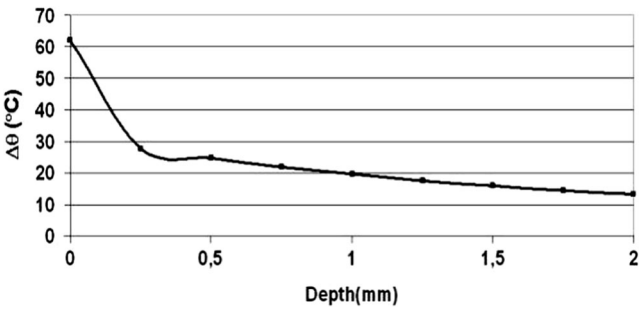

Fig. 7 Example of temperature gradient for $\boldsymbol{v_c}$=80 m/min and $\boldsymbol{f}$=0.17 mm/rev

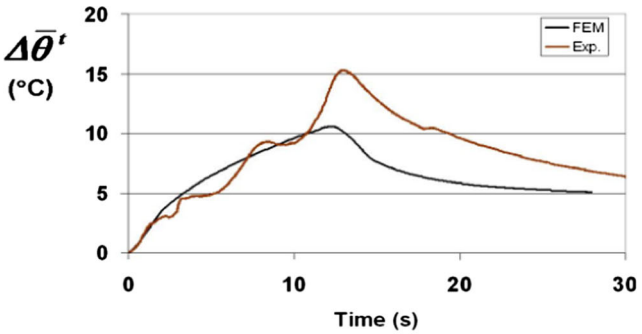

(a) v_c = 80 m/min and f =0.17 mm/rev.

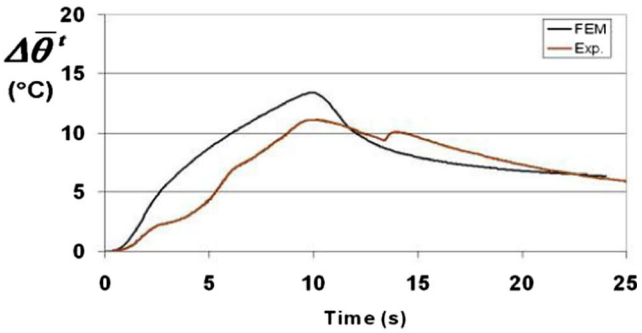

(a) v_c = 100 m/min and f =0.17 mm/rev.

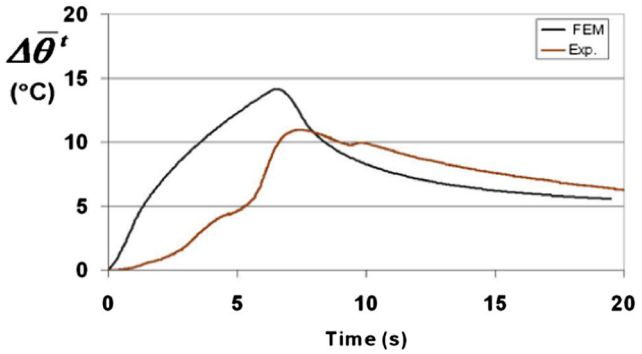

(a) v_c = 150 m/min and f =0.17 mm/rev.

Fig. 8 Comparison between experimental and simulated average temperature

and the second according to the Eq. (14) as follows:

$$\Delta\bar{\theta}^t = \frac{\sum_{i=1}^{N} \left(\Delta\theta_i^t\right)}{N} \tag{14}$$

Where $\Delta\bar{\theta}^t$ is the average temperature rise at the time t, $\Delta\theta_i^t$ is the temperature at time t from the thermocouple i, and N is the number of thermocouples. The parameter $\Delta\bar{\theta}^t$ gives the curve of temperature increase overall the workpiece and should be a fair comparison between both techniques to describe the temperature.

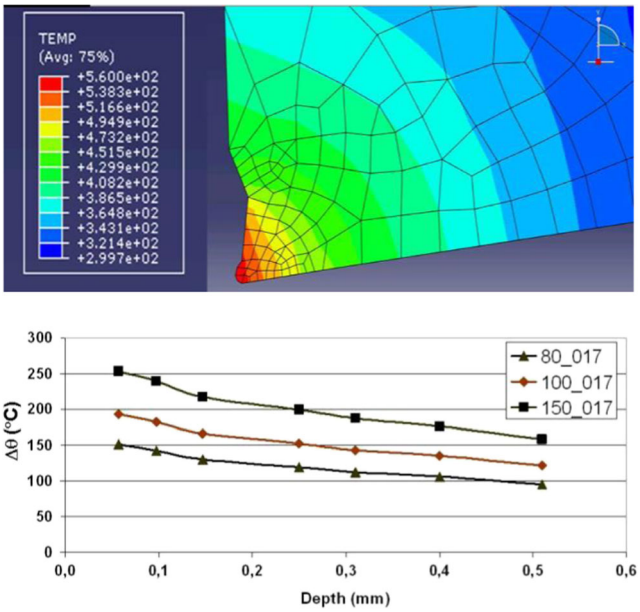

Fig. 9 Temperature distribution on the cutting edge

4 Results and discussions

Figure 5 shows the experimental results of the convection coefficient (h) as a function of temperature rise at the surface.

There was a tendency of h to increase with the surface rise in temperature, which is expected according to [22]. Since the expected rise in surface temperature on the experimental milling operation is closer to the highest values in Fig. 5, the value used for the simulations was 125 W/m^2. Figure 6 shows examples of experimental and simulated curves of temperature rise versus time for the same cutting conditions.

Thermocouples T2, T5, T5 and T11 were excluded due to failure during the experiments. There were also differences in response time, which is due to variations on their fabrication and the distances from the milled surface. Although the holes were precisely at the same distance from the surface, small variations on the thermocouple positioning resulted in variation on the measured temperature because the gradient is high near the surface. Figure 7 shows the temperature curves as a function of depth, at the center of the workpiece.

Computation time for both models took between 5 and 8 h, using a INTEL XEON 3.2 GHz, 32 GB RAM, 8 processors workstation. Figure 8 shows the averaged temperature rise at the workpiece.

The results indicate a relatively good agreement between the experimental and FEM-simulated results. The highest temperatures in both techniques disagree significantly in absolute values, but the experimental values have also some measurements errors. The time in which the peak occurs cannot be fairly compared because the synchronization is very difficult, since the time when the cutting edge touches the workpiece could be precisely determined. Besides that, the

response time of the thermocouples presents, in itself, additional problems.

Figure 9 shows the results of the temperature distribution on the cutting edge, using the same technique.

5 Conclusions

From the present work, the following can be concluded:

- The use of a hybrid approach with explicit algorithm for chip formation and implicit one for heat propagation proved to be very adequate to simulate heat in end milling operations.
- The adopted models allowed the simulation of a complete end milling operation in less than 6 h of computer time. Therefore, it is possible to simulate complex machining process, such as metal cutting, through advanced general-purpose commercial codes [Umbrello].
- The comparison of simulated results with experimental ones showed a good agreement in terms of average temperature rise in the workpiece. Furthermore, the difference appears also includes experimental error on measurements of the temperature and simplifications imposed in the FEM modeling.
- Temperature inside the cutting edge could also be obtained and can be used to help in coating analysis and design.

References

1. Krause F-L, Kimura F, Kjellberg T, Lu SC-Y, van der Wolf, Alting L, ElMaraghy HA, Eversheim W, Iwata K, Suh NP, Tipnis VA, Week M (1993) A.C.H, product modelling. CIRP Ann Manuf Technol 42(2): 695–706. doi:10.1016/S0007-8506(07)62532-3
2. Merchant ME (1998) An interpretive look at 20th century research on modeling of machining. Mach Sci Technol 2(2):p157–p163
3. van Luttervelt CA, Childs THC, Jawahir IS, Klocke F, Venuvinod PK, Altintas Y, Armarego E, Dornfeld D, Grabec I, Leopold J, Lindstrom B, Lucca D, Obikawa T, Shirakashi, Sato H (1998) Present situation and future trends in modelling of machining operations progress report of the CIRP Working Group 'Modelling of Machining Operations'. CIRP Ann Manuf Technol 47(2):587–626. doi:10.1016/S0007-8506(07)63244-2
4. Coelho RT, Ng E, Elbestalwi M (2007) Tool wear when turning hardened AISI 4340 with coated PCBN tools using finishing cutting conditions. Intl J Mach Tools Manuf 47:263–272
5. Umbrello D (2008) Finite element simulation of conventional and high speed machining of Ti6Al4V alloy. J Mater Process Technol 196(1–3):79–87. doi:10.1016/j.jmatprotec.2007.05.007
6. Sandstrom DR, Hodowany JN (1998) Modeling the physics of metal cutting in high-speed machining. Mach Sci Technol 2(2):343–353
7. Marusich TD, Ortiz M (1995) Modelling and simulation of high-speed machining. Int J Numer Methods Eng 38(21):3675–3694. doi: 10.1002/nme.1620382108
8. Filice L, Micari F, Rizzuti S, Umbrello D (2008) Dependence of machining simulation effectiveness on material and friction modelling. Mach Sci Technol 12(3):370–389
9. Sartkulvanich P, Altan T (2005) Effects of flow stress and friction models in finite element simulation of orthogonal cutting—a sensitivity analysis. Mach Sci Technol (Issue 9):1–26. doi:10.1081/MST-200051211
10. Shi J, Liu CR (2004) The influence of material models on finite element simulation of machining. J Manuf Sci Eng 126(4):849–857. doi:10.1115/1.1813473
11. Anurag S, Guo YB, Horstemeyer MF (2009) The effect of materials testing modes on finite element simulation of hard machining via the use of internal state variable plasticity model coupled with experimental study. Comput Struct 87(5–6):303–317. doi:10.1016/j.compstruc.2009.01.001
12. Bil H, Kılıç SE, Tekkaya AE (2004) A comparison of orthogonal cutting data from experiments with three different finite element models. Int J Mach Tools Manuf 44(9):933–944. doi:10.1016/j.ijmachtools.2004.01.016
13. Bao Y, Wierzbicki T (2005) On the cut-off value of negative triaxiality for fracture. Eng Fract Mech 72(7):1049–1069. doi:10.1016/j.engfracmech.2004.07.011
14. Wierzbicki T, Bao Y, Lee Y-W, Bai Y (2005) Calibration and evaluation of seven fracture models. Int J Mech Sci 47(4–5):719–743. doi:10.1016/j.ijmecsci.2005.03.003
15. Shirakashia T, Obikawa T (1998) Recent progress and some difficulties in computational modeling of machining. Mach Sci Technol 2(2): 277–301. doi:10.1080/10940349808945672
16. Ceretti E, Filice L, Umbrello D, Micari F (2007) ALE simulation of orthogonal cutting: a new approach to model heat transfer phenomena at the tool-chip interface. CIRP Ann Manuf Technol 56(1):69–72. doi:10.1016/j.cirp.2007.05.019
17. Umbrello D, Filice L, Micari F, Settineri L (2005) A simple model for predicting the thermal flow on the tool in orthogonal cutting process. Proceedings "8th CIRP International Workshop on Modeling of Machining Operations", Chemnitz (Germany), 10–11 May, pp. 191–197
18. Bergman TL, Lavine AS, Incropera FP, DeWitt DP (1985) Fundaments of heat and mass transfer, School of Mechanical Engineering Purdue University. John Wiley & Sons, Inc
19. Guo YB, Anurag S, Jawahir IS (2009) A novel hybrid predictive model and validation of unique hook-shaped residual stress profiles in hard turning. CIRP Ann Manuf Technol 58(1):81–84. doi:10.1016/j.cirp.2009.03.110
20. Pabst R, Fleischer J, Michna J (2010) Modelling of the heat input for face-milling processes. CIRP Ann Manuf Technol 59(1):121–124. doi:10.1016/j.cirp.2010.03.062
21. Davies MA, Ueda T, M'Saoubi R, Mullany B, Cooke AL (2007) On the measurement of temperature in material removal processes. CIRP Ann Manuf Technol 56(2):581–604. doi: 10.1016/j.cirp.2007.10.009
22. Fleischer J, Pabst R, Kelemen S (2007) Heat flow simulation for dry machining of power train castings. CIRP Ann Manuf Technol 56(1): 117–122. doi:10.1016/j.cirp.2007.05.030